Measurement of $\alpha_4\beta_2$ Nicotinic Acetylcholine Receptors with [^{123}I]5-I-A-85380 SPECT

Masahiro Fujita, Gilles Tamagnan, Sami S. Zoghbi, Mohammed S. Al-Tikriti, Ronald M. Baldwin, John P. Seibyl, and Robert B. Innis

Departments of Psychiatry, Diagnostic Radiology, and Pharmacology, Yale University School of Medicine and VA Connecticut, West Haven, Connecticut

Nicotinic acetylcholine receptors (nAChRs) play an important role in tobacco dependence and a potential therapeutic role in neuropsychiatric disorders such as Alzheimer's disease. [^{123}I]5-iodo-3-[2(*S*)-2-azetidinylmethoxy]pyridine (5-I-A-85380) is a new SPECT tracer that labels $\alpha_4\beta_2$ nAChRs. The purpose of this study was to assess the usefulness of this tracer to measure regional nAChR binding in baboon brain using both a bolus/kinetic paradigm and also a bolus plus constant infusion/equilibrium paradigm. **Methods:** A pair of bolus/kinetic and bolus plus constant infusion/equilibrium studies was performed in each of 3 isoflurane-anesthetized baboons. Bolus studies were performed by intravenous injection of 191–226 MBq [^{123}I]5-I-A-85380 and image acquisition for 289–367 min. The data were analyzed with 1- and 2-tissue compartment models. Bolus plus constant infusion/equilibrium studies were performed by a bolus injection (74–132 MBq) followed by a 468- to 495-min infusion with a bolus/infusion ratio (B/I) of 4.8–5.0 h. The distribution volumes in the thalamus were measured in these 2 paradigms. To study whether the cerebellum was appropriate as a receptor-poor region, displacement studies were done in 2 baboons using the B/I paradigm with subcutaneous injection of (−)-cytisine (0.8 and 1.0 mg/kg). **Results:** The kinetics of this tracer was best described by the 1-tissue compartment model. The 2-compartment model showed poor identifiability of rate constants. The total (specific plus nondisplaceable compartments) distribution volumes (V_T') agreed between bolus and B/I paradigms (average percentage difference in V_T', 16.8%). (−)-Cytisine (0.8 and 1.0 mg/kg) displaced 70% and 72% of the radioactivity in the thalamus and 36% and 55% in the cerebellum, respectively, indicating that the latter was not appropriate as a receptor-poor region. **Conclusion:** These results show the feasibility of quantifying $\alpha_4\beta_2$ nAChRs using [^{123}I]5-I-A-85380 and support the use of V_T' as an appropriate outcome measure.

Key Words: nicotinic receptors; 3-[2(*S*)-2-azetidinylmethoxy]pyridine; SPECT; compartment analysis; equilibrium analysis

J Nucl Med 2000; 41:1552–1560

Nicotinic acetylcholine receptors (nAChRs) belong to the superfamily of ligand-gated ion channels and mediate neurotransmission throughout the central and peripheral nervous systems. There is great interest in studying these receptors in humans because they appear to play an important role in tobacco dependence and may also have therapeutic usefulness in Alzheimer's disease. The effects of nicotine are mediated through its initial actions at nAChRs, and smoking has been reported to increase this receptor subtype ~2-fold in both animals and humans (*1*,*2*). The classical cholinergic hypothesis of Alzheimer's disease derives from the degeneration and loss of cholinergic neurons in the basal forebrain (*3*). A reduction of nAChRs has been reported in this disorder (*4*), and nicotine has been reported to improve cognitive function (*5*) and protect against β-amyloid cytotoxicity (*6*).

Imaging studies of nAChRs have been hampered by the lack of a tracer that is suitable for in vivo imaging. Nicotine itself has been labeled with ^{11}C and used as a PET tracer in humans (*7*). However, its usefulness was significantly impaired by high nonspecific uptake (*7*). Epibatidine is a potent ligand with subnanomolar affinity for several subtypes of nAChRs, including the $\alpha_4\beta_2$ subtype (the most predominant subtype in brain (*8*)) and the $\alpha_3\beta_4$ subtype (present in sympathetic ganglia (*9*)). nAChRs have been successfully imaged in vivo using ^{18}F- (*10*) and ^{11}C-labeled (*11*) epibatidine analogs for PET and ^{123}I labeling for SPECT (*12*). However, because of its high toxicity (*13*), caution must be exercised in human studies using epibatidine-related compounds. Recently, the azetidine derivative (*R*)-5-[2-azetidinylmethoxy]-2-chloro-pyridine (ABT-594) has been developed, which has affinity comparable with that of epibatidine at nAChRs (K_i [inhibition constant], ~40 pmol/L) but with much less toxicity (*14*,*15*). The lower toxicity of ABT-594 is presumably associated with its low affinity at the $\alpha_3\beta_4$ receptor and much lower cardiovascular effects mediated through the sympathetic nervous system.

An analog of ABT-594, 3-[2(*S*)-2-azetidinylmethoxy]pyridine (A-85380), has been labeled with ^{123}I (5-iodo-3-[2(*S*)-azetidinylmethoxy]pyridine (5-I-A-85380) (Fig. 1) (*16*–*19*) and ^{18}F (*11*,*15*) and shown to be suitable for in vivo imaging. Ex vivo studies using rodents showed high specific uptake in the thalamus and superior colliculus, moderate uptake in the hippocampus and striatum, and low uptake in the cerebellum (*17*,*18*,*20*), which is compatible with the distribution of nAChRs (*21*–*23*). SPECT (*16*,*19*) and PET (*15*) studies

Received Sep. 30, 1999; revision accepted Feb. 16, 2000.
For correspondence or reprints contact: Masahiro Fujita, MD, PhD, VA Connecticut/116A2, 950 Campbell Ave., West Haven, CT 06516.

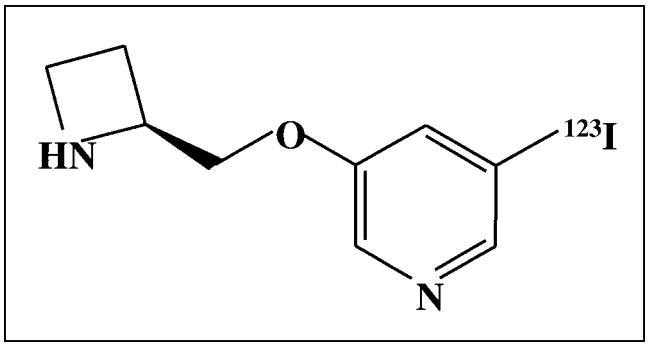

FIGURE 1. Structure of [^{123}I]5-I-A-85380.

using nonhuman primates showed high specific uptake in the thalamus. However, quantitation of nAChRs with this PET tracer was reported only in abstract form (*24*).

The main purpose of this work was to investigate the feasibility of measuring the distribution volumes of [^{123}I]5-I-A-85380 in a nonhuman primate by applying bolus/kinetic and bolus plus constant infusion/equilibrium paradigms in the same animals and cross-validating the results with the 2 different paradigms. Quantitation of receptor densities can be simplified if a receptor-poor region is available. Using the data in a receptor-poor region, a specific-to-nondisplaceable ratio can be measured without using blood data (*25,26*) and can be used to estimate receptor densities. The density of cholinergic innervation is low in the cerebellum. Although rodent (*18*) and rhesus monkey (*16*) studies showed the absence of specific uptake in the cerebellum, a report using baboons indicated the presence of specific uptake in the cerebellum (*19*). Therefore, displacement studies were performed to determine whether the cerebellum could be used as a receptor-poor region for quantitation of receptor binding potential (BP).

MATERIALS AND METHODS

Radiolabeling

The radiotracer [^{123}I]5-I-A-85380 was prepared by iododestannylation of the *t*-butoxycarbonyl protected trialkylstannyl precursor 5-trimethylstannyl-3-[1-*t*-butoxycarbonyl-2(*S*)-azetidinylmethoxy]pyridine in the presence of chloramine-T (*19*). In a typical procedure, to a vial containing 740 MBq no-carrier-added sodium [^{123}I]iodide in 100 μL dilute (~0.1 mol/L) NaOH (Nordion International, Vancouver, British Columbia, Canada) contained in a 1-mL conical serum vial was added, in the following order, 20 μL 1 mol/L HCl, 300 μg stannyl precursor dissolved in 100 μL ethanol, and 50 μg chloramine-T (as trihydrate) in 50 μL H_2O. After 20–30 min at room temperature, 100 μg $NaHSO_3$ in 100 μL H_2O was added, and the headspace of the vial was purged with N_2 (gas) into a charcoal trap. Then a 400-μL mobile phase and 100 μL saturated $NaHCO_3$ were added, and the mixture was purified by high-performance liquid chromatography (HPLC) (C_{18} Novapak, 4.6 × 250 mm; Waters, Mississauga, Ontario, Canada; methanol/H_2O/triethylamine, 65:35:0.2, 1.0 mL/min; retention time of 5-I-A-85380, 10.2 min) and formulated in 5% ethanol/normal saline as described (*27*). The labeling yield averaged 66.3% ± 18.6% (mean ± SEM; n = 16) but the isolated yield of final product was 48.4% ± 17.5% because of adsorption of radiotracer to the membrane filters used for final filtration (Acrodisc 13; Gelman Science, Ann Arbor, MI). Radiochemical purity averaged 97.9% ± 2.8% (mean ± SD; n = 9). Sterility was confirmed by lack of growth in 2 media, fluid thioglycollate at 35°C and soybean-casein digest at 25°C, for 2 wk.

SPECT Studies

Eight SPECT scanning experiments were performed in 3 ovariectomized female baboons (16–17 kg). One pair of bolus/kinetic and bolus plus constant infusion/equilibrium studies was performed in all 3 baboons, with intervals between the experiments of 14, 30, and 14 d for baboons 1, 2, and 3, respectively. SPECT data were acquired with a multislice brain-dedicated CERASPECT camera (Digital Scintigraphics, Waltham, MA) with a resolution in all 3 axes of ~12-mm full width at half maximum measured with an ^{123}I line source in a 20.0-cm H_2O-filled cylindric phantom. Data were obtained as 64 slices, each on a 128 × 128 matrix with a voxel size of 1.67 × 1.67 × 1.67 mm.

Fasted animals were immobilized with ketamine (10 mg/kg, intramuscularly) and then anesthetized with 2% isoflurane. Glycopyrrolate (4 μg/kg, intramuscularly), a long-acting peripheral anticholinergic drug known not to cross the blood–brain barrier, was administered at the beginning of the study to decrease respiratory and digestive secretions. The interval between ketamine administration and the injection of [^{123}I]5-I-A-85380 was a minimum of 2 h to allow the animal's physiology to stabilize under isoflurane anesthesia. Three fiducial markers, each filled with 75–175 kBq ^{123}I, were glued on the left and 2 were glued on the right side of the animal's head at the level of the canthomeatal plane to control positioning in the gantry before tracer injection and to check posthoc for movement during the experiment. The head was immobilized with a beanbag, which hardens on evacuation (Olympic Medical, Seattle, WA). Body temperature was maintained between 35.8°C and 37.5°C in all experiments with heated water blankets. Lactated Ringer's solution was infused intravenously at a rate of 8.8 mL/h/kg body weight.

Bolus/Kinetic Study. [^{123}I]5-I-A-85380 (191, 222, and 226 MBq) was intravenously injected as a single bolus over 30 s and followed by serial image acquisitions of 10 × 4 min, 5 × 7 min, 12 × 10 min, and every 15 min thereafter. The durations of the studies were 289, 367, and 365 min, respectively. Plasma samples (0.5 mL) were obtained from an artery in the leg every 20 s for the first 2 min using a Harvard 250-001 peristaltic pump (Harvard Apparatus, South Natick, MA). Subsequent samples (0.75 mL) were obtained manually at 4.5, 7.5, 10.5, 15, 20, 30, 60, 90, 120, 180, and 240 min.

Bolus Plus Constant Infusion/Equilibrium Study. [^{123}I]5-I-A-85380 (130, 132, and 73.6 MBq) was intravenously injected as a single bolus over 30 s and followed immediately by a continuous infusion of [^{123}I]5-I-A-85380 using a computer-controlled Gemini PC-1 pump (IMED, San Diego, CA). The bolus/infusion ratio (B/I) was set at 4.8–5.0 h, which means the infused dose over 4.8–5.0 h corresponded to the dose of the bolus injection. The durations of the studies were 468, 494, and 495 min. Venous samples (3 mL) were obtained every 30 min starting at 4.5 h after the bolus injection.

Displacement Study with (−)-Cytisine. Displacement studies were performed in baboons 1 and 2 with (−)-cytisine (0.8 and 1.0 mg/kg subcutaneously, respectively; Sigma Chemical Co., St. Louis, MO). The experiments were performed as described above, with the exception that a higher B/I of 7.1 h was applied for baboon

2 because the prior use of a B/I of 5.0 h yielded a late time to equilibrium. The doses of the bolus were 85.4 and 105 MBq. To check equilibrium before (−)-cytisine administration, venous samples (3 mL) were obtained every 30 min starting at 3.5 h after the bolus injection.

MRI

To identify brain regions, MRI scans of 1.5-mm contiguous slices were obtained with a 1.5-T Signa device (General Electric Medical Systems, Milwaukee, WI). Axial images were acquired using a spoiled gradient-recalled acquisition in the steady-state sequence with repetition time, 25 ms; echo time, 6 ms; flip angle, 30°; number of excitations, 2; matrix, 256 × 256; and field of view, 16 cm.

Plasma Analysis

Plasma tracer concentration was determined by γ counter assay of 50-μL aliquots (CompuGamma 1282; LKB-Wallach, Turku, Finland), and the metabolite fraction was determined by acetonitrile denaturation followed by HPLC (*28*,*29*). The plasma free fraction (f_1) was measured with ultracentrifugation as described (*30*). To control for day-to-day variability in the assay, 1 aliquot from a pooled sample of plasma obtained from healthy human volunteers was processed with each experiment as a standard. f_1 measured in each study was corrected for interassay variability using the f_1 measured in the standard ($f_{1\ std}$) and the average of the standard measurement in the 8 studies ($f_{1\ ave}$, 0.386) according to $[(f_1 \times f_{1\ ave})/f_{1\ std}]$. The average of $f_{1\ std}$ was 0.524.

In bolus studies, clearance was calculated by dividing injected dose by the area under the curve in plasma. The area under the curve was obtained from the areas during the first 2 min and triexponential fitting after 2 min. In bolus plus infusion studies, clearance was calculated by dividing the infusion rate by the parent level in plasma.

Image Analysis

SPECT images were reconstructed with a Butterworth filter (cutoff, 0.75 cm; order, 10) on a CERASPECT workstation (Digital Scintigraphics). Attenuation correction was performed assuming uniform attenuation equal to that of H_2O (0.15 cm^{-1}) within an ellipse drawn around the skull. Image analyses were performed on MEDx 3.1 (Multimodality Radiological Image Processing; Sensor System, Inc., Sterling, VA). Tissues other than brain and orbits were manually deleted from the MR image. A summed SPECT image created from all image acquisitions in each study was coregistered with the edited MR image using a surface registration algorithm (*31*). Volumes of interest (VOIs) were placed on the thalamus (4 slices, 2.8–3.3 mL) and the cerebellum (3 slices, 2.8–3.1 mL) in the coregistered MR image in reference to an atlas of the baboon brain (*32*). To minimize the influence of scattered radiation from the high uptake in the thalamus, the VOI was placed over the external portions of the cerebellar cortex, which corresponded to approximately half of the total volume of the cerebellum in the analyzed slices. Average activity (cpm/mL) for each VOI was converted to kBq/mL using a calibration factor (37.5 Bq/cpm) measured with a 10.5-cm-diameter distributed source filled with ^{123}I solution, acquired, and reconstructed using the same protocol.

Derivation of Rate Constants and Distribution Volumes

Bolus/Kinetic Study. One- and a 2-tissue compartment models were tested to analyze time–activity curves. In the 1-compartment model, brain activity was described by a single compartment; in the 2-compartment model, activity was described separately by nondisplaceable and specifically bound compartments. Rate constants (K_1, k_2, k_2', k_3, and k_4) were defined as described (*33*). In the 1-compartment model,

$$V_T = \frac{K_1}{k_2' f_1}, \qquad \text{Eq. 1}$$

where V_T is the distribution volume for the single tissue compartment. In the 2-compartment model, V_T is described separately by the distribution volumes in the nondisplaceable compartment (V_2) and specific binding compartment (V_3).

$$V_2 = \frac{K_1}{k_2 f_1}, \qquad \text{Eq. 2}$$

$$V_3 = \frac{K_1 k_3}{k_2 k_4 f_1} = \frac{B_{max}'}{K_d} = BP, \qquad \text{Eq. 3}$$

$$V_T = \frac{K_1(1 + k_3/k_4)}{k_2 f_1}, \qquad \text{Eq. 4}$$

where B_{max}' is unoccupied receptor density. Although the definition of K_1 is the same in these 2 models, that of k_2 and k_2' is different. That is, k_2 refers to the transfer from the nondiplaceable compartment, and k_2' refers to the transfer from the total tissue compartment (*33*). In the 1-compartment model, variables are generally identified well because the number of variables is small. However, V_3 (BP) cannot be calculated in this model. Because $V_T = V_2 + V_3$, intersubject variability of V_2 must be small compared with that of V_3 so that V_T reflects differences in V_3. On the contrary, although V_3 can be obtained in the 2-compartment model, identifiability of variables may not be good because of the larger number of variables.

V_i' was defined as

$$V_i' = f_1 V_i. \qquad \text{Eq. 5}$$

Because f_1 is already an inverse factor in the calculation of V_i, these definitions essentially imply that V_i values are expressed relative to the free fraction of radiotracer in plasma and that V_i' values are expressed relative to the total concentration of radiotracer in plasma. The reliability of V_i' is generally higher than that of V_i because of error in the measurement of f_1.

In nonlinear least-squares analysis for the 1-compartment model, V_T' was treated as a variable in place of k_2' to determine the identifiability of the outcome measure (Eqs. 1 and 5). In a similar way, in the 2-compartment model, V_2' and V_3' were treated as variables in place of k_2 and k_4, respectively (Eqs. 2, 3, and 5). The 2-compartment model was solved in the following 2 ways. First, fitting was performed without constraint. Second, V_2 was constrained to be the same in both the thalamus and cerebellum, and $V_2' = K_1/k_2$ was coupled between these regions.

Nonlinear least-squares analysis was performed on the VOI-generated time–activity data using PMOD 1.20 (*34*). Parameters were estimated using the Marquardt algorithm (*35*) with constraints restricting parameters (except time shift) to positive values. Each model configuration was implemented to account for the contribution from activity in the cerebral blood volume and for time offset or shift between the plasma input function measured from the leg arterial samples and the actual arterial input to the brain. Cerebral blood volume was assumed to be 5% of brain volume. Each data point was weighted by $1/y_i$, where y_i is the counting rate (kBq/mL).

The SEs of the rate constants were given by the diagonal of the

covariance matrix (*36*) and expressed as a percentage of the rate constants (coefficient of variation [%COV]). The F-statistic (*37*) was applied to compare goodness of fit in the 1- and 2-compartment models.

V_T and V_T' were also calculated by the Logan's plot (*38*) using PMOD 1.20 (*34*).

Bolus Plus Infusion/Equilibrium Study. Under equilibrium conditions, V_T and V_T' were calculated by dividing activities in the thalamus by free and total (free plus protein bound) parent tracer in plasma, respectively.

RESULTS

Plasma Analysis

In bolus studies, plasma activity peaked between 20 and 80 s and decreased rapidly to 3%–17% of the peak within 20 min (Figs. 2A and B). HPLC analysis separated a polar metabolite, a lipophilic metabolite, and the parent tracer with retention times of 5, 8–9, and 13–14 min, respectively. The tracer was quickly metabolized and represented 48%–50% and 20%–26% of total plasma activity at 10.5 and 30 min, respectively (Fig. 2C). In bolus plus infusion studies (including the 2 displacement experiments), total plasma activity, parent metabolite level, and a polar metabolite level were stable with average changes of −1.3%/h to 0.0%/h, −1.5%/h to +0.8%/h, and +0.1%/h to +1.4%/h, respectively, starting at 208–390 min to the end of study (Fig. 3A). A lipophilic metabolite was also stable with an average change of −1.5%/h to +0.2%/h starting at 270–420 min, except for 1 study that showed a decrease of −7.2%/h. During these stable periods, fractions of the parent, polar, and lipophilic metabolites were 15.9%–36.7%, 50.8%–70.7%, and 12.5%–21.4%, respectively. Clearance of the parent tracer was 24.7–74.4 L/h (mean, 37.6 L/h) in 8 experiments, including 2 displacement studies.

Brain Analysis

Bolus/Kinetic Studies. The thalamus was the brain region with the highest brain uptake (Fig. 4). Ex vivo studies in rodents have shown moderate uptake in the hippocampus and striatum (*17,18,20*), structures that are located close to the thalamus. Because of the limited resolution of SPECT and the small size of the baboon brain, hippocampal and striatal VOIs might contain significant scattered activity

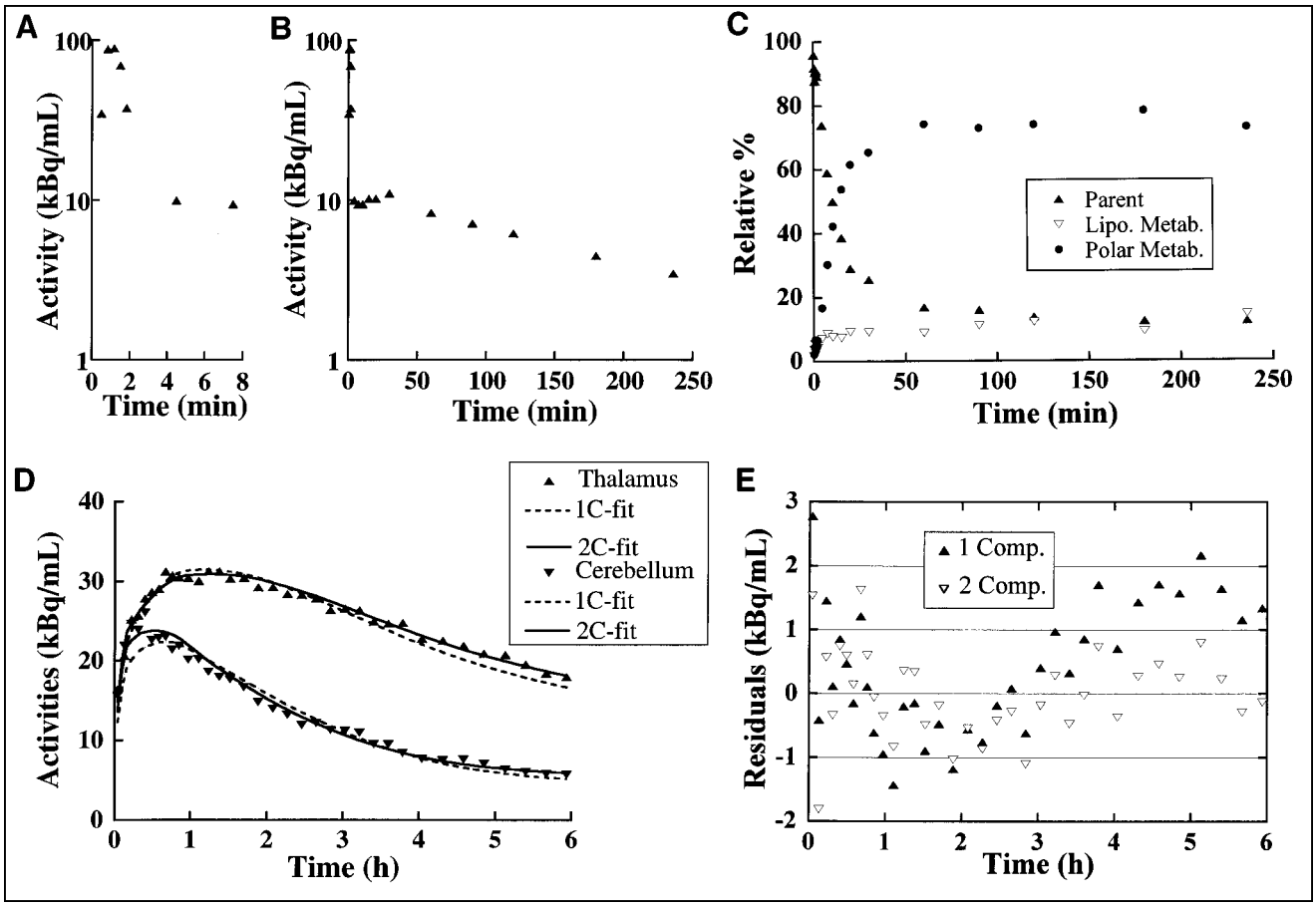

FIGURE 2. Bolus/kinetic study of baboon 3. Injected dose of [^{123}I]5-I-A-85380 was 226 MBq. (A and B) Plasma activity. (C) Fractions of parent tracer and lipophilic (Lipo.) and polar metabolites (Metab.) in plasma show rapid metabolism of tracer. (D) Time–activity curves in thalamus and cerebellum with nonlinear least-squares fitting, using 1-compartment (1C) and 2-compartment (2C) models. Fitting by coupled 2-compartment model is shown in graph. (E) Residuals (measured − fitted values) of thalamic curve in (D). 1 Comp. = 1 compartment; 2 Comp. = 2 compartment. Two-compartment model shows better fitting.

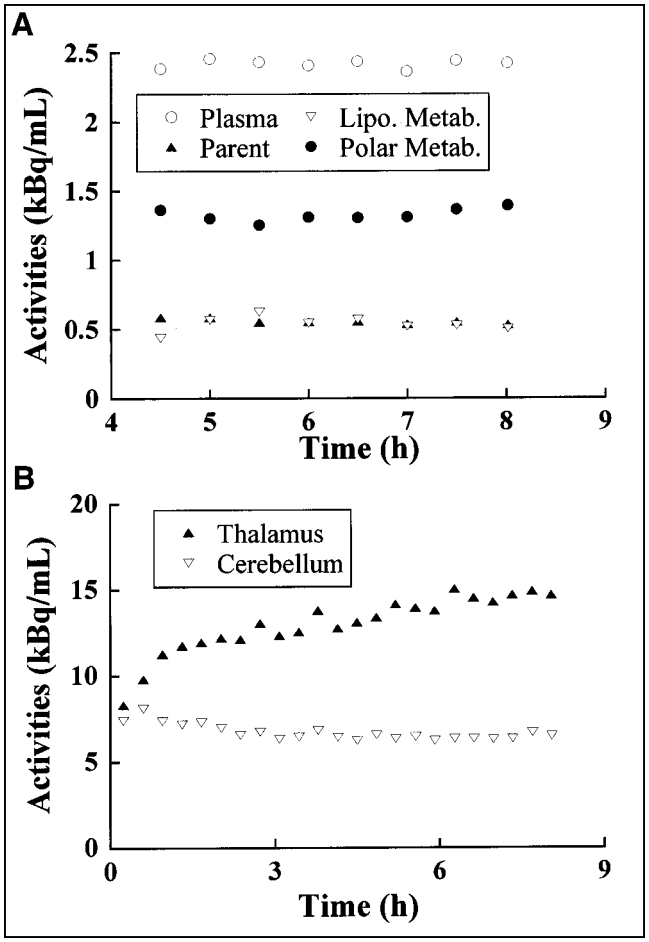

FIGURE 3. Bolus plus infusion/equilibrium study in baboon 3. Bolus dose of [^{123}I]5-I-A-85380 was 73.6 MBq, with B/I of 4.8 h. (A) Plasma data show stable levels in total activity, parent tracer, and lipophilic (Lipo.) and polar metabolite (Metab.) levels. (B) Time–activity curves in thalamus and cerebellum show achievement of stable brain activities, consistent with equilibrium receptor binding conditions in brain.

from the thalamus. Therefore, VOI analyses were performed only in the thalamus and cerebellum.

In 3 bolus studies, the peak uptake occurred at 34, 86, and 75 min and at 18, 29, and 24 min in the thalamus and the cerebellum, respectively (Fig. 2D). The peak total thalamic uptake was 1.38%–1.66% injected dose/100 mL brain.

Bolus Plus Infusion/Equilibrium Studies. In 3 bolus/infusion studies, the uptake in the thalamus achieved stable levels (average changes, −0.1%/h to +0.1%/h) starting at 373–399 min (Fig. 3B). The uptake in the cerebellum reached stable levels (average change, −1.7%/h to +0.03%/h) earlier than that in the thalamus, starting at 163–224 min.

Displacement Studies. Displacement studies were performed in baboons 1 and 2 with (−)-cytisine (0.8 and 1.0 mg/kg, respectively) using a bolus plus constant infusion of radiotracer (Fig. 5). Stable brain uptake was achieved in baboon 1, with −0.3%/h in the thalamus and −0.6%/h in the cerebellum after 123 and 139 min, respectively. However, brain activities were not as stable in baboon 2, presumably because of a high B/I, with −6.6%/h in the thalamus and +0.7%/h in the cerebellum during the last 3 15-min acquisitions before (−)-cytisine administration. Parent tracer concentrations in the plasma were stable throughout both studies, with changes of +0.2%/h and +0.8%/h from 208 and 240 min, respectively. (−)-Cytisine administration showed a maximum displacement within ~2 h. In baboon 1, the data from 139 min to the acquisition before cytisine administration was used as baseline. In baboon 2, 3 time points before the administration were used as baseline. In both studies, the last 3 time points were used to measure the displacement. The displacement was 70% and 72% in the thalamus, respectively, and 36% and 55% in the cerebellum, respectively. Because of the deviation from equilibrium conditions, displacement in the thalamus might have been overestimated in baboon 2. The apparent displacements of cerebellar activity were caused either by true specific uptake in the cerebellum or by the influence from displaced activity in the thalamus. In either case, the cerebellar VOI would not be appropriate to use as a receptor-poor region for compartmental modeling analysis.

Derivation of Rate Constants and Distribution Volumes

Bolus/Kinetic Studies. In the 1-compartment model, the 2 variables K_1 and V_T' were well identified in all 3 animals with a %COV of 3.5–5.1 and 0.15–0.21 in the thalamus and 2.1–2.5 and 0.2–1.2 in the cerebellum (Table 1).

The 2-compartment model was solved in 2 ways: unconstrained and coupled. Because the cerebellar VOI showed displaceable activity, the 2-compartment model was also applied in this region. Unconstrained fitting showed poor identifiability in both of the 2 tissue compartments (V_2' and V_3') in the thalamus with a %COV of 29–37 and 6.1–49, respectively. The coupling of V_2' between the thalamus and cerebellum significantly improved the identifiability of the

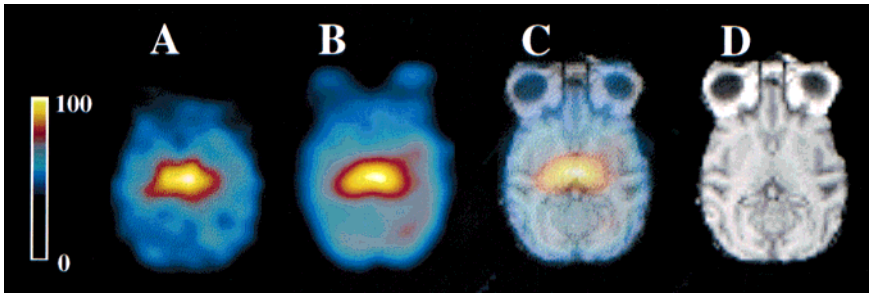

FIGURE 4. Bolus/kinetic study of baboon 2 with injection of 222 MBq. (A) SPECT image acquired from 122 to 132 min. (B) Summation image created from all acquisitions during 6-h study. (D) Coregistered MR image. (C) Fused image created from (B) and (D) shows highest brain uptake in thalamus.

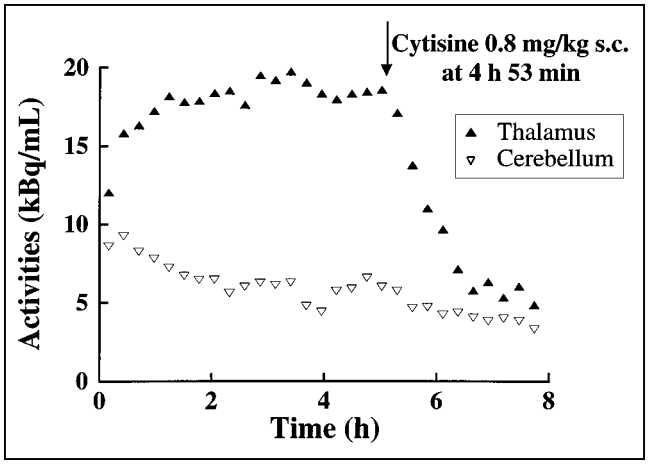

FIGURE 5. Displacement by (−)-cytisine (0.8 mg/kg subcutaneously) in baboon 1. Apparent displacement was 72% and 36% in thalamus and cerebellum, respectively.

distribution volumes in these 2 tissue compartments, with a %COV of 1.5–4.8 and 2.1–4.8 for V_2' and V_3', respectively, in the thalamus (Table 2). Because it provided greater identifiability, only the coupled model was evaluated further. Although the coupled model identified V_2' and V_3' well in the thalamus, V_3' in the cerebellum was not identified well in animals 1 and 2, with a %COV of 36 and 33, respectively, and k_3 in the cerebellum was poorly identified in all 3 animals (Table 2). K_1 values by the 1- and the coupled 2-compartment models were reasonably close, although the values by the latter were about 10% greater (Tables 1 and 2).

Goodness of fit of the 2-compartment model as measured by the F-statistic was significantly better than that of the 1-compartment model in all animals ($P < 0.001$). However, in the 2-compartment model, parameters were not identified well without coupling V_2' between the thalamus and cerebellum, and the parameters were not well identified in the latter region. On the contrary, the 1-compartment model identified all parameters well in the 2 regions in all animals. Therefore, the 1-compartment model, not the 2-compartment model, should be used to analyze bolus studies.

V_T and V_T' in the thalamus were obtained by the 1- and 2-compartment models (Eqs. 1, 4, and 5) and Logan's plot. V_T was 58.2–87.0 mL/mL and V_T' was 23.8–36.0 mL/mL (Table 3). The 3 methods applied in bolus studies showed virtually identical values for V_T and V_T' in each animal.

Bolus Plus Infusion/Equilibrium Studies. V_T and V_T' were calculated from the data in which both thalamic activities and plasma parent levels were stable. The results were V_T = 74.4–133 and V_T' = 27.2–46.1 mL/mL (Table 3).

Comparison Between Bolus and Infusion Paradigms. Because the 3 methods applied in bolus studies showed almost identical V_T and V_T' values, average values by these methods were compared with the results in bolus plus infusion studies in each animal (Table 3). The distribution volumes obtained in the bolus studies were smaller than those in the bolus plus infusion studies in all animals. The variability (difference of the 2 methods divided by the average) was small, with an average of 16.8% in V_T', indicating that the quantification was reasonably accurate. The larger variability of 27.9% in V_T was consistent with the expected uncertainty introduced with an additional measured variable.

TABLE 1
Least-Squares Estimates of Rate Constants for 1-Compartment Model

Animal no.	Thalamus			Cerebellum		
	K_1 (mL/mL/min)	V_T' (mL/mL)	SS	K_1 (mL/mL/min)	V_T' (mL/mL)	SS
1	0.136 (3.5)	35.1 (0.15)	61.7	0.119 (2.1)	16.7 (1.2)	55.0
2	0.138 (4.3)	24.5 (0.20)	44.3	0.130 (2.5)	7.6 (0.2)	53.4
3	0.129 (5.1)	25.0 (0.21)	43.0	0.116 (2.1)	10.0 (0.2)	96.8

SS = sum of squares.
Numbers in parentheses indicate identifiability of rate constants expressed as %COV.

DISCUSSION

The feasibility of quantifying [^{123}I]-5-I-A-85380 in vivo binding to $\alpha_4\beta_2$ nAChRs in nonhuman primate brain was assessed with bolus/kinetic and bolus plus constant infusion/equilibrium paradigms. The displacement of the cerebellar uptake by (−)-cytisine (36% and 55%) indicated that this region was not appropriate as a receptor-poor region. In the bolus studies, poor identifiability of variables by the 2-compartment model indicated that the kinetics of this tracer was better described by the 1-compartment model. Good agreement in V_T' between the bolus and infusion paradigms indicated that the quantification was accurate.

Uptake in Cerebellum

If a receptor-poor region is available, quantitation of receptor densities can be simplified by applying reference tissue models (*25*,*26*). Can the cerebellum, which receives a sparse cholinergic innervation, be used as a receptor-poor region? Previous reports have been contradictory, with 2 showing no specific uptake in mice (*18*) and rhesus monkeys (*16*) and 1 showing 59% displacement with (−)-cytisine in baboons (*19*). In this study, 36% and 55% displacement was measured with (−)-cytisine administration in 2 animals. Two factors must be considered as the source of this apparent displacement. One is the influence of the high uptake in the thalamus and the other is the presence of specific binding.

Baseline V_T' was 50.2 and 30.6 mL/mL in the thalamus and 16.7 and 11.6 mL/mL in the cerebellum in animals 1 and 2, respectively. Measured displacement was 70% and 72% in the thalamus and 36% and 55% in the cerebellum in these animals. These results can be analyzed with the assumption that no true displacement occurred in the cerebellum, but it reflected scattered activity from the thalamus. Under this

TABLE 2
Least-Squares Estimates of Rate Constants for Coupled 2-Compartment Model

Animal no.	V_2' (mL/mL)	Thalamus K_1 (mL/mL/min)	Thalamus k_3 (min^{-1})	Thalamus V_3' (mL/mL)	Thalamus SS	Cerebellum K_1 (mL/mL/min)	Cerebellum k_3 (min^{-1})	Cerebellum V_3' (mL/mL)	Cerebellum SS
1	15.4 (4.8)	0.136 (9.7)	0.173 (649)	20.4 (2.4)	56.7	0.129 (13)	0.00076 (107)	3.13 (36)	28.2
2	7.0 (4.3)	0.167 (9.1)	0.041 (22)	18.8 (2.1)	21.4	0.137 (3.1)	0.00102 (82)	0.72 (33)	37.1
3	8.9 (1.5)	0.145 (12)	0.040 (24)	18.1 (4.8)	17.0	0.135 (25)	0.00113 (91)	2.13 (5.5)	34.4

SS = sum of squares.
Numbers in parentheses indicate identifiability of rate constants expressed as %COV. Values of K_1/k_2 were coupled in thalamus and cerebellum.

assumption, 51% (36 × 100/70) and 76% (55 × 100/72) of the total counts measured in the cerebellum at baseline must be caused by the activities in the thalamus, and 17% and 29% of the activities in the thalamus must be detected by the VOI placed in the cerebellum. Considering the distance between the thalamus and cerebellum, these numbers are unlikely. In addition, a PET study using [^{18}F]2-fluoro-A-85380 in baboons also showed a 46% reduction in cerebellar uptake induced by (−)-cytisine (*15*). Although ^{18}F and ^{123}I labeling may change the properties of the tracer, PET has higher resolution and less influence of scatter than SPECT.

[^{123}I]5-I-A-85380 binds to the $\alpha_4\beta_2$-type nAChRs with high affinity (*14*) and may have high affinity for other subtypes with a β_2 subunit (K. Kellar, PhD, personal communication, May 1999). In rats, [^{125}I]5-I-A-85380 has shown no specific binding in the cerebellum (*18*), where the level of α_4 nAChR messenger RNA (mRNA) was low (*39*) and the level of β_2 mRNA was high in the Purkinje layer (*39*). In humans, the expression of α_4 mRNA in the cerebellum was even higher than that in the cerebral cortices (*40*). Therefore, there are species differences in the distribution of nAChRs. For human studies the binding of [^{123}I]5-I-A-85380 in the cerebellum should be studied in vitro using human tissue, which is free of the confounding factors in imaging studies such as limited resolution and scattered radiation. If the human cerebellum does not show specific binding in vitro, this region may be used as a receptor-poor region in the larger human brain and by applying a scatter-correction algorithm.

Compartmental Description of Thalamic Uptake

V_3 (BP) can be obtained by the 2- but not by the 1-compartment model in a bolus/kinetic paradigm. Because a receptor-poor region was not available in baboon, V_3 could not be obtained in the bolus plus infusion/equilibrium paradigm. Therefore, it was important to study whether the uptake in the thalamus was reasonably described by the 2-compartment model. In the 2-compartment model, k_3 in the thalamus was poorly identified in 1 animal, and parameters were poorly identified in the cerebellum in all animals, which was coupled in the fitting. Therefore, the uptake of this tracer was not well described by the 2-compartment model, and V_T and V_T', which can be obtained by the 1-compartment model and Logan's plot, should be used as a measure of receptor densities. As described in the Materials and Methods, the usage of V_T and V_T' as a measure of BP is confounded by the intersubject variability in V_2 and V_2', and, if the parameters are well identified, it is preferable to use V_3 or V_3'. However, these measures were not reliable in this study. In the larger human brains, other receptor-rich regions such as the hippocampus and striatum may be measured independently of the thalamus. In this case, the 2-compartment model may provide reliable V_3 values by coupling V_2 among a few receptor-rich regions such as the thalamus, hippocampus, and striatum.

V_T and V_T' were obtained in both bolus/kinetic and bolus plus infusion/equilibrium paradigms in each animal. These 2 paradigms should theoretically show identical distribution volumes even if the experiments are performed separately. V_T' showed good agreement, indicating that the results were

TABLE 3
Total Distribution Volumes in Thalamus

Animal no.	V_T (mL/mL) 1-comp. fits	V_T (mL/mL) 2-comp. fits	V_T (mL/mL) Logan	V_T (mL/mL) Equilibrium	V_T' (mL/mL) 1-comp. fits	V_T' (mL/mL) 2-comp. fits	V_T' (mL/mL) Logan	V_T' (mL/mL) Equilibrium
1	84.9	86.6	87.0	132.8	35.1	35.8	36.0	46.1
2	60.8	63.8	59.0	75.3	24.5	25.7	23.8	30.2
3	58.2	62.8	60.9	74.4	25.0	26.9	26.1	27.2

comp. = compartment; Logan = Logan's plot (*38*).
Free and total (free + protein bound) parent levels in plasma were used to calculate V_T and V_T', respectively.

accurate. Bigger discrepancies in V_T indicate errors in f_1 measurement. However, in all animals, bolus plus infusion studies showed a greater V_T', which may indicate a bias. A couple factors should be considered. The scattered radiation from adjacent areas detected in the thalamus would be greater in bolus studies because the initial uptake reflects mainly blood flow but not receptor binding. This factor would lead to greater values in bolus studies, which is the opposite trend of the present results. During infusion for several hours, the level of lipophilic metabolite reached a level similar to that of the parent tracer. This accumulated metabolite, though less lipophilic than the parent tracer, may contribute to the greater V_T' in bolus plus infusion studies. Although V_T' in the thalamus was 17% greater in equilibrium studies, there was no such trend in V_T' of the cerebellum (bolus, 7.3–18.5 mL/mL; bolus plus infusion, 11–15.4 mL/mL), where receptor density is low, although it may not be negligible. Therefore, 1 possibility is that the metabolite binds to the receptor. If a similar trend is found in human studies, the chemical identity and the property of the lipophilic metabolite need to be studied.

CONCLUSION

This study has shown that it is feasible to quantify nAChRs using [^{123}I]5-I-A-85380 in nonhuman primates. V_T' was appropriate as a measure of the uptake. Further studies should be performed in humans to develop a method of quantification that is feasible for patients and also to study the uptake in the regions close to the thalamus, such as the hippocampus and striatum, by applying scatter correction.

ACKNOWLEDGMENTS

The authors thank Cyrill Burger, PhD, Piotr Rudnicki, MS, Krzysztof Mikolajczyk, MS, and Michal Grodzki, MS, for providing PMOD 1.20; Luis Amici and Quinn Ramsby for technical assistance; and John L. Musachio, PhD, for helpful discussion. This work was supported by the Connecticut/Massachusetts VA Mental Illness Research Education and Clinical Center and Transdisciplinary Tobacco Research Center P50 DA84733.

REFERENCES

1. Schwartz RD, Kellar KJ. Nicotinic cholinergic receptor binding sites in brain: regulation in vivo. *Science.* 1983;220:214–216.
2. Perry DC, Dávila-García MI, Stockmeier CA, Kellar KJ. Increased nicotinic receptors in brains from smokers: membrane binding and autoradiography studies. *J Pharmacol Exp Ther.* 1999;289:1545–1552.
3. Coyle JT, Price DL, DeLong MR. Alzheimer's disease: a disorder of cortical cholinergic innervation. *Science.* 1983;219:1184–1190.
4. London ED, Ball MJ, Waller SB. Nicotinic binding sites in cerebral cortex and hippocampus in Alzheimer's dementia. *Neurochem Res.* 1989;14:745–750.
5. White HK, Levin ED. Four-week nicotine skin patch treatment effects on cognitive performance in Alzheimer's disease. *Psychopharmacology.* 1999;143: 158–165.
6. Kihara T, Shimohama S, Urushitani M, et al. Stimulation of α4β2 nicotinic acetylcholine receptors inhibits β-amyloid toxicity. *Brain Res.* 1998;792:331–334.
7. Nybäck H, Halldin C, Ahlin A, Curvall M, Eriksson L. PET studies of the uptake of (S)- and (R)-[^{11}C]nicotine in the human brain: difficulties in visualizing specific receptor binding in vivo. *Psychopharmacology.* 1994;115:31–36.
8. McGehee DS, Role LW. Physiological diversity of nicotinic acetylcholine receptors expressed by vertebrate neurons. *Ann Rev Physiol.* 1995;57:521–546.
9. Cimino M, Marini P, Fornasari D, Cattabeni F, Clementi F. Distribution of nicotinic receptors in cynomolgus monkey brain and ganglia: localization of alpha 3 subunit mRNA, alpha-bungarotoxin and nicotine binding sites. *Neuroscience.* 1992;51:77–86.
10. Horti A, Scheffel U, Stathis M, et al. Fluorine-18-FPH for PET imaging of nicotinic acetylcholine receptors. *J Nucl Med.* 1997;38:1260–1265.
11. Horti AG, Scheffel U, Kimes AS, et al. Synthesis and evaluation of N-[^{11}C]methylated analogues of epibatidine as tracers for positron emission tomographic studies of nicotinic acetylcholine receptors. *J Med Chem.* 1998;41:4199–4206.
12. Musachio J, Horti A, London E, Dannals R. Synthesis of a radioiodinated analogue of epibatidine: (+/−)-exo-2-(2-iodo-5-pyridyl)-7-azabicyclo[2.2.1]-heptane for *in vitro* and *in vivo* studies of nicotinic acetylcholine receptors. *J Labeled Compd Radiopharm.* 1997;39:39–48.
13. Sullivan J, Decker M, Brioni J, et al. (+/−)-Epibatidine elicits a diversity of in vitro and in vivo effects mediated by nicotinic acetylcholine receptors. *J Pharmacol Exp Ther.* 1994;271:624–631.
14. Sullivan JP, Donnelly-Roberts D, Briggs CA, et al. A-85380 [3-(2(S)-azetidinylmethoxy) pyridine]: in vitro pharmacological properties of a novel, high affinity alpha 4 beta 2 nicotinic acetylcholine receptor ligand. *Neuropharmacology.* 1996;35:725–734.
15. Valette H, Bottlaender M, Dollé F, et al. Imaging central nicotinic acetylcholine receptors in baboons with [^{18}F]fluoro-A-85380. *J Nucl Med.* 1999;40:1374–1380.
16. Chefer SI, Horti AG, Lee KS, et al. *In vivo* imaging of brain nicotinic acetylcholine receptors with 5-[^{123}I]iodo-A-85380 using single photon emission computed tomography. *Life Sci.* 1998;25:PL355–PL360.
17. Musachio JL, Scheffel U, Finley PA, et al. 5-[I-125/123]iodo-3(2(*S*)-azetidinylmethoxy)pyridine, a radioiodinated analog of A-85380 for *in vivo* studies of central nicotinic acetylcholine receptors. *Life Sci.* 1998;22:PL351–PL357.
18. Vaupel DB, Mukhin AG, Kimes AS, Horti AG, Koren AO, London ED. *In vivo* studies with [^{125}I]5-I-A-85380, a nicotinic acetylcholine receptor radioligand. *NeuroReport.* 1998;9:2311–2317.
19. Musachio JL, Villemagne VL, Scheffel UA, et al. Synthesis of an I-123 analog of A-85380 and preliminary SPECT imaging of nicotinic receptors in baboon. *Nucl Med Biol.* 1999;26:201–207.
20. Horti AG, Scheffel U, Koren AO, et al. 2-[^{18}F]fluoro-A-85380, an in vivo tracer for the nicotinic acetylcholine receptors. *Nucl Med Biol.* 1998;25:599–603.
21. Clarke PB, Schwartz RD, Paul SM, Pert CB, Pert A. Nicotinic binding in rat brain: autoradiographic comparison of [^{3}H]acetylcholine, [^{3}H]nicotine, and [^{125}I]-alpha-bungarotoxin. *J Neurosci.* 1985;5:1307–1315.
22. London ED, Waller SB, Wamsley JK. Autoradiographic localization of [^{3}H]nicotine binding sites in the rat brain. *Neurosci Lett.* 1985;53:179–184.
23. Swanson LW, Simmons DM, Whiting PJ, Lindstrom J. Immunohistochemical localization of neuronal nicotinic receptors in the rodent central nervous system. *J Neurosci.* 1987;7:3334–3342.
24. Yokoi F, Musachio J, Hilton J, et al. Kinetic modeling of nicotinic acetylcholine receptor ligand, [C11]A-84543 in baboon PET study [abstract]. *J Nucl Med.* 1999;40(suppl):263P.
25. Ichise M, Ballinger JR, Golan H, et al. Noninvasive quantification of dopamine D2 receptors with iodine-123-IBF SPECT. *J Nucl Med.* 1996;37:513–520.
26. Lammertsma AA, Hume SP. Simplified reference tissue model for PET receptor studies. *Neuroimage.* 1996;4:153–158.
27. Baldwin RM, Zea-Ponce Y, Zoghbi SS, et al. Evaluation of the monoamine uptake site ligand [^{123}I]methyl 3β-(4-iodophenyl)tropane-2β-carboxylate ([^{123}I]β-CIT) in nonhuman primates: pharmacokinetics, biodistribution, and SPECT brain imaging coregistered with MRI. *Nucl Med Biol.* 1993;20:597–606.
28. Zoghbi SS, Baldwin RM, Seibyl JP, et al. Pharmacokinetics of the SPECT benzodiazepine receptor radioligand [^{123}I]iomazenil in human and nonhuman primates. *Int J Rad Appl Instrum B.* 1992;19:881–888.
29. Zoghbi SS, Tamagnan G, Fujita M, et al. Metabolism of 5-[I-123]-iodo-3-(2(3)-azetidinylmethoxy)pyridine, a nicotinic acetylcholine receptor imaging agent, in non-human primates. *J Labeled Compd Radiopharm.* 1999;42(suppl 1):666–668.
30. Gandelman MS, Baldwin RM, Zoghbi SS, Zea-Ponce Y, Innis RB. Evaluation of ultrafiltration for the free fraction determination of single photon emission computed tomography (SPECT) tracers: β-CIT, IBF, and iomazenil. *J Pharm Sci.* 1994;83:1014–1019.
31. Pelizzari CA, Chen GTY, Spelbring DR, Weichselbaum RR, Chen CT. Accurate three dimensional registration of CT, PET, and/or MR images of the brain. *J Comput Assist Tomogr.* 1989;13:20–26.
32. Riche D, Hantraye P, Guibert B, Naquet R, Loch'h C, Mazière M. Anatomical atlas of the baboon's brain in the orbito-meatal plane used in experimental positron emission tomography. *Brain Res Bull.* 1988;20:283–301.
33. Laruelle M, Baldwin RM, Rattner Z, et al. SPECT quantification of [^{123}I]iomazenil binding to benzodiazepine receptors in nonhuman primates. I. Kinetic

modeling of single bolus experiments. *J Cereb Blood Flow Metab.* 1994;14:439–452.
34. Burger C, Mikolajczyk K, Grodzki M, Rudnicki P, Szabatin M, Buck A. JAVA tools quantitative post-processing of brain PET data [abstract]. *J Nucl Med.* 1998;39(suppl):277P.
35. Bevington PR. *Data Reduction and Error Analysis for the Physical Sciences.* New York, NY: McGraw-Hill; 1969.
36. Carson RE. Parameter estimation in positron emission tomography. In: Phelps ME, Mazziotta JC, Schelbert HR, eds. *Positron Emission Tomography and Autoradiography: Principles and Applications for the Brain and Heart.* New York, NY: Raven Press; 1986:347–390.
37. Hawkins RA, Phelps ME, Huang S-C. Effects of temporal sampling, glucose metabolic rates, and disruptions of the blood-brain barrier on the FDG model with and without a vascular compartment: studies in human brain tumors with PET. *J Cereb Blood Flow Metab.* 1986;6:170–183.
38. Logan J, Fowler JS, Volkow ND, et al. Graphical analysis of reversible radioligand binding from time-activity measurements applied to [N-^{11}C-methyl]-(−)cocaine PET studies in human subjects. *J Cereb Blood Flow Metab.* 1990;10:740–747.
39. Wada E, Wada K, Boulter J, et al. Distribution of alpha2, alpha3, alpha4, and beta2 neuronal nicotinic receptor subunit mRNAs in the central nervous system: a hybridization histochemical study in the rat. *J Comp Neurol.* 1989;284:314–335.
40. Hellström-Lindahl E, Mousavi M, Zhang X, Ravid R, Nordberg A. Regional distribution of nicotinic receptor subunit mRNAs in human brain: comparison between Alzheimer and normal brain. *Mol Brain Res.* 1999;66:94–103.